Colloids and Surfaces B: Biointerfaces 81 (2010) 304–312

Contents lists available at ScienceDirect

Colloids and Surfaces B: Biointerfaces

journal homepage: www.elsevier.com/locate/colsurfb

Optimized immobilization of gold nanoparticles on planar surfaces through alkyldithiols and their use to build 3D biosensors

Anne-Laure Morel[a,b], Rose-Marie Volmant[a,b], Christophe Méthivier[a,b], Jean-Marc Krafft[a,b], Souhir Boujday[a,b,*], Claire-Marie Pradier[a,b]

[a] UPMC Univ Paris 6, UMR CNRS 7197, Laboratoire de Réactivité de Surface, F75005 Paris, France
[b] CNRS, UMR 7197, Laboratoire de Réactivité de Surface, F75005 Paris, France

ARTICLE INFO

Article history:
Received 22 February 2010
Received in revised form 28 May 2010
Accepted 8 July 2010
Available online 15 July 2010

Keywords:
Biosensor
Hexanedithiol
Gold nanoparticles
Self-assembled monolayers
AFM
PM-IRRAS
XPS

ABSTRACT

This paper describes a controlled way to immobilize gold nanoparticles on planar gold surfaces and the use of the resulting 3D platform to build up a 3D biosensor. The surface was first functionalized by grafting hexanedithiol, this molecule has 2 thiol end groups, which enables its chemical grafting to planar gold while retaining a free thiol group to attach nanoparticles. This step was optimized by varying experimental parameters such as solvent, temperature and immersion time. The grafting was monitored by polarization modulation infrared reflection absorption spectroscopy (PM-IRRAS) and X-ray photoelectron spectroscopy (XPS). The high resolution XPS sulfur peak made clear the existence of two contributions, S bound to gold and free S, thus led us to determine the optimal conditions to graft hexanedithiol in an extended conformation. 15 nm spherical gold nanoparticles were then immobilized on the resulting surface and their presence was evidenced by surface enhanced Raman spectroscopy (SERS) and atomic force microscopy (AFM). The resulting gold layer was used to build up a 3D biosensor by grafting protein A (PrA), rabbit immunoglobulin (rIgG), and bovine serum albumin (BSA), respectively. Each step was characterized by PM-IRRAS then compared to the results on planar gold surface. Despite the small size of particles and their rather low density on the planar surface, the amount of immobilized proteins, starting from PrA, was almost doubled. The amount of rIgG fixed on the 3D layer was also significantly increased (~4 times higher than on planar surfaces), however accompanied by a slight decrease of their accessibility, checked by assaying the recognition of a secondary IgG. This work demonstrates the feasibility and interest of building arrays of nanoparticles to immobilize molecular receptors; it also shows that controlling the conditions of elaboration of the biosensor at each step is determining for optimizing the number of molecular receptors.

1. Introduction

Biosensors are small detection devices made of a biological recognition element immobilized on transducing surface [1]. Immunosensors are a sub-class where the recognition element is an antibody [2]. These devices are widely used to detect and quantify several types of targets such as toxins, bacteria or pollutants provided that specific antibodies are available [3–6]. The crucial challenge in immunosensing field is sensitivity that depends drastically on the amount of antibodies and their accessibility [7] (and references therein). Because of its conductivity, reflectivity, and robustness, gold is often used as transducing surface. It is well-known that gold reacts with alkylthiols that spontaneously form more or less ordered self-assembled monolayers (SAMs). Formation of SAMs has been widely studied by surface characterization techniques [8] and their building on gold surfaces allows controlling the amount and orientation of the antibodies [6,9,10]. However, the use of planar gold as transducing surface may lead to a limited number of accessible antibodies. The challenge is thus to increase the amount of antibodies while preserving their accessibility. One possible way is building 3D gold layer using nanosized gold nanoparticles. Nanosize gold particles have been successfully used to enhance the sensitivity of biomolecular detection assays, either by improving the antibody immobilisation [11,12], or by increasing the sensitivity of some specific detection techniques like electrochemical techniques, surface plasmon resonance (SPR), quartz crystal microbalance (QCM) or surface enhanced Raman scattering (SERS) for instance. One of the first studies reporting the use of Np-labeled antibody and signal enhancement was performed by Lyon et al. [13]. They reported a 25-fold increases of sensitiv-

* Corresponding author at: Laboratoire de Réactivité de Surface, UMR CNRS 7197, Université Pierre et Marie Curie- Paris VI, 4 Place Jussieu, 75252 Paris cedex 05, France. Tel.: +33 144276001; fax: +33 144276033.
E-mail address: souhir.boujday@upmc.fr (S. Boujday).

0927-7765/$ – see front matter © 2010 Elsevier B.V. All rights reserved.
doi:10.1016/j.colsurfb.2010.07.021

ity by using simple gold Np-labeled antibodies in a direct format immunosensor.

Gold Np have been currently used to detect immunologic reactions by electron microscopy or electrochemical methods; a gold Np layer, assembled on a gold electrode, was shown to facilitate electron transfers occurring in an enzymatic reaction, thus enhancing a glucose oxidase-based immunosensor [14]. More recently a remarkable cartography of cancer markers in the brain was obtained by scanning tunneling microscopy thanks to the use of Nps; Au Np-labeled antibodies were reacted on top of an antibody–target complex, in a sandwich type immunoassay; this configuration, combined with SPR detection improved the sensitivity compared to the label-free SPR analysis by a 10^3 factor [15]. In order to circumvent the long antibody labeling procedure, Ko et al. directly deposited a colloidal solution of 30 nm diameter Np on an $-NH_2$-terminated SAM on a SPR chip; antibody probes were then grafted via a gold binding peptide-PrA fusion protein; a 10-fold sensitivity increase was observed in the detection of *Salmonella typhimurium* [11].

Gold nanoparticles have also been used to enable detection of antigen coupling by SERS; as an example, Lin et al. co-immobilized antibodies and a SERS reporter molecule on 20 nm diameter gold Np and used them to selectively bind to immobilised antibodies; a sensitivity down to the pg/mL was obtained [16]. All these recent examples witness the rapid development of the use of Np for biosensor technologies, and point out the importance of controlling their immobilization on sensors surfaces. The immobilization of gold nanoparticles on planar surfaces is often carried out using an amine terminated layer, expected to bind nanoparticles through "electrostatic interactions" [17,18]. Covalent binding of gold nanoparticles could be obtained using thiol terminated layer. Typically, on gold surfaces, one can use alkyldithiols. Such molecules, containing two sulfur extremities are supposed to bind to planar gold surface while leaving the second sulfur free to further grafting. Hexanedithiol was previously utilized in this purpose [19]. Several grafting procedures can be found, mainly using ethanol as solvent [19,20] but also toluene [21] or water [22]. To the best of our knowledge, no chemical characterizations were performed to control this crucial step and correlate it to the configuration of grafted hexanedithiols. The only example of chemical characterization of the S–Au bond for this molecule was performed by XPS using capping of nanoparticles in solutions then their depositing on quartz surface without building of SAM [21]. In this context, we propose to build controlled layers of alkyldithiols with respect to their amount and orientation on planar gold and use them to immobilize gold nanoparticles to form 3D biosensing platforms. Our objectives are: first to optimise the experimental conditions of surface functionalization and gold nanoparticles grafting by investigating parameters like solvent, temperature, and immersion time; second to evaluate the geometric effect of the resulting 3D platforms, i.e. measure the increase of both the number of antibody probes and of their accessibility regardless of the effect on the detection technique sensitivity. The latter point will be the subject of a forthcoming work.

2. Experimental

2.1. Materials

1-Mercapto-11-undecanoic acid (MUA), N-hydroxysuccinimide (NHS), N-1-(3-dimethylaminopropyl)-N′-ethylcarbodiimide hydrochloride (EDC) were purchased from Aldrich (France). Rabbit IgG (rIgG), goat anti-rabbit IgG (anti-rIgG), goat serum, bovine serum albumin, (BSA) and recombinant protein A (PrA) were purchased from Sigma. All solvents were reagent-grade and used without any further purification.

Gold surfaces are constituted of glass substrates (11 mm × 11 mm), coated successively with a 25 å thick layer of chromium and a 200 nm thick layer of gold, were purchased from Arrandee (Werther, Germany). The gold-coated substrates were annealed in a butane flame to ensure a good crystallinity of the topmost layers and rinsed in a bath of absolute ethanol during 15 min before adsorption.

2.2. SAMs formation

Gold-coated sensor chips, after being treated in a flame and cleaned in ethanol,were immersed in 10 mL of a 10 mM solution of hexanedithiol (DT; Aldrich) in water or ethanol. Two immersion temperatures (room temperature and 4 °C), two solvents (water and ethanol) and several immersion times (from 1 to 12 h) were investigated in order to evidence a possible influence of the immersion conditions on the monolayer quality. In each case, the substrates were washed with the same volume of water or EtOH and dried under nitrogen flow.

2.3. Gold nanoparticles synthesis

Gold nanoparticles were prepared according to the Turkevich method [17,23]. 50 mL of a 5×10^{-2} M solution were prepared from a commercial stock $HAuCl_4$ solution (Aldrich, France). Then, 10 mL of 1% citrate solution were added under stirring, and under reflux. After 10 min, the reflux was stopped but stirring continued during 10 min. The resulting solution was characterized by UV–vis spectroscopy in transmission mode, and by scanning electron.

2.4. Covalent immobilization of gold nanoparticles

Gold substrates were immersed in 10 mL of the gold nanoparticule solution at room temperature and during 1 or 3 h, or at 4 °C during 3 h then washed twice in ultrapure water.

2.5. Immunosensor elaboration

Planar and 3D gold substrates were immersed in 10 mM solutions of 1-Mercapto-11-undecanoic acid (MUA) in ethanol; on gold nanoparticles, the objective was to replace citrate ligands by the acid-terminated thiol. After 3 h, the substrates were washed 3 times in the same volume of EtOH and dried under nitrogen flow. The resulting acid-terminated layers were activated, by formation of NHS ester functions using a previously optimized procedure [24]: a solution of NHS (60 mM) and EDC (30 mM) in water for 1 h 30 min then, immersed in a solution of PrA (50 mg L^{-1}) in PBS pH 7.4. After 1 h, substrates were washed three times with PBS. Then, a microdrop of a 50 mg L^{-1} solution of BSA (Sigma) in PBS was deposited for 30 min to block non-specific binding sites. After rinsing 3 times in PBS, model rIgGs (50 mg L^{-1} in PBS) were added by depositing a drop onto the substrates during 1 h and washed again in PBS. Antibodies' accessibility was checked by adding secondary anti-rIgG (50 mg L^{-1} in PBS, 1 h) then washing 3 times in PBS.

2.6. Characterization techniques

2.6.1. PM-IRRAS

PM-IRRAS spectra were recorded on a commercial Thermo-Scientific (France) Nexus spectrometer. The external beam was focused on the sample with a mirror, at an optimal incident angle of 75°. A ZnSe grid polarizer and a ZnSe photoelastic modulator, modulating the incident beam between p- and s-polarizations

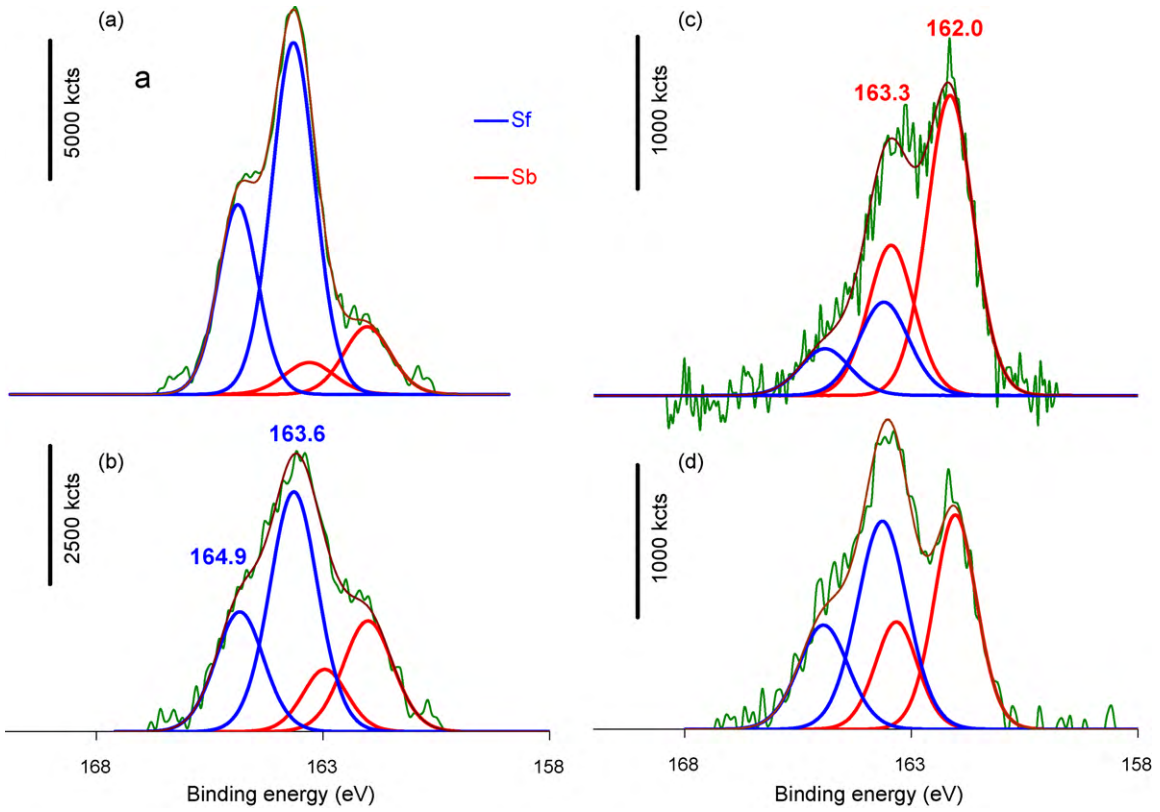

Fig. 1. XPS spectra for sulfur peak at various experimental conditions: (a) 12 h in water at room temperature, (b) 12 h in ethanol at room temperature, (c) 3 h in ethanol at room temperature, (d) 3 h in ethanol at 4 °C, Sb and Sf being used for sulfur bound to gold and free sulfur respectively.

(HINDS Instruments, PEM 90, modulation frequency = 37 kHz), were placed prior to the sample. The light reflected at the sample was then focused onto a nitrogen-cooled MCT detector. The presented spectra result from the sum of 128 scans recorded at a 8 cm^{-1} resolution. The PM-IRRAS signal is given by the differential reflectivity $\Delta R/R = (R_p - R_s)/(R_p + R_s)$ [25,26]. IR sensors were glass substrates (11 mm × 11 mm) successively coated with a 50 nm thick layer of chromium and a 200 nm thick layer of gold. These substrates were purchased from Arrandee (Werther, Germany). Before chemical functionalization, they were annealed in a flame, then rinsed in ultrapure water and dried under nitrogen flow.

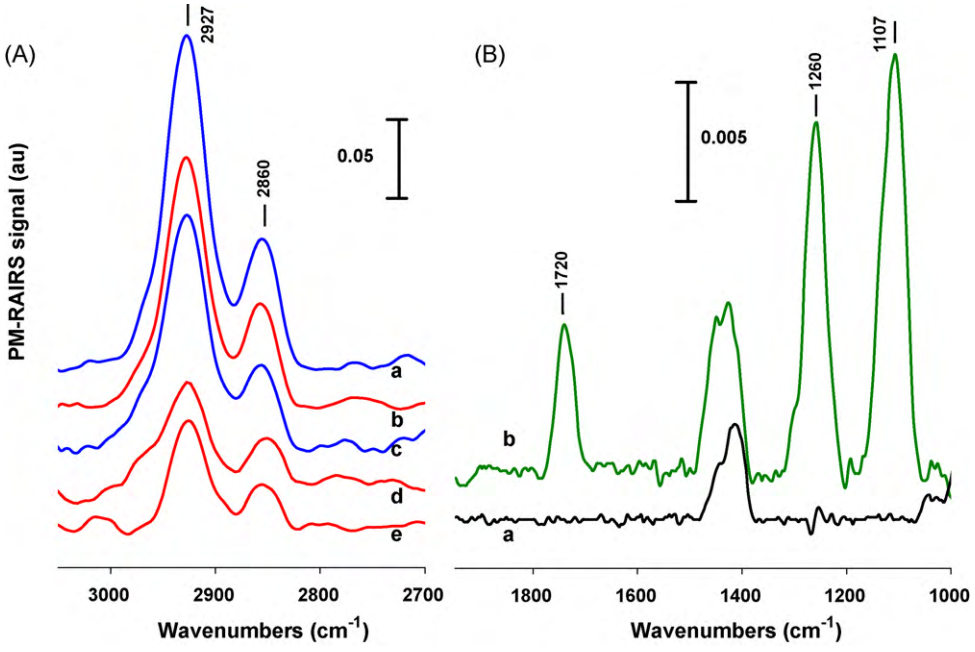

Fig. 2. PM-IRRAS spectra. (A) Upon hexanedithiols grafting at various experimental conditions: (a) 12 h in water at room temperature, (b) 12 h in ethanol at room temperature, (c) 3 h in water at room temperature, (d) 3 h in ethanol at room temperature, (e) 3 h in ethanol at 4 °C. (B) (a) Upon hexanedithiols grafting-3 h in ethanol at 4 °C (another region of wavenumbers for the spectrum d), (b) after gold nanoparticles grafting on (a).

Table 1
XPS and PM-IRRAS data obtained upon grafting hexanedithiol at various conditions.

Solvent	Time (h)	Temperature	CH bands area (au)	S/Au	S bound/S free
Water	3	RT	0.81	0.031	0.25
	12	RT	2.2	0.049	0.3
Ethanol	1	RT	0.35	–	–
	3	RT	0.43	0.006	2.2
	12	RT	0.83	0.018	0.45
	24	RT	0.87	–	–
	3	4 °C	0.52	0.010	1.2

2.6.2. XPS

Analyses were performed with a PHOIBOS 100 X-ray photoelectron spectrometer from SPECS GmbH (Germany) with an Mg Kα X-ray source ($h\nu$ = 1253.6 eV), operating at 10^{-10} Torr or less, in a "fixed analyzer transmission" analysis mode with a 7 mm × 20 mm entrance slit, leading to a resolution of 0.1 eV. A 20 eV pass energy for the survey scan and 10 eV pass energy for the S 2p region were applied. Binding energies were calibrated against the Au $4f_{7/2}$ binding energy of the substrate that was set at 84.0 eV, leading to a CC, CH carbon peak at 285 eV. The spectra were fitted using Casa XPS software (version 2.3.13, Casa Software, UK).

2.6.3. AFM

The AFM images of dried surfaces were recorded using a commercial di Caliber AFM microscope from VEECO Instruments Inc. In order to avoid tip and sample damages, topographic images were taken in the non-contact dynamic mode also known as tapping® mode. Silicon nitride tips (resonance frequency of ~278 kHz, spring constant of 40–80 N/m) have been used. Images were obtained at a constant speed of 2 Hz with a resolution of 512 × 512 pixels each. The raw data were processed using the imaging processing software di SpmLabAnalysis v.7.0. from Veeco Instruments Inc.

2.6.4. SERS

Surface enhanced Raman scattering spectra were recorded in the 100–3450 cm^{-1} range on a commercial modular Raman spectrometer (Model HL5R of Kaiser Optical Systems, Inc.). It displays a high-powered near-IR laser diode working at 785 nm. Before taking the spectra, an optical microscope (Olympus, objective: 100×) was used to focus the laser beam.

3. Results and discussion

3.1. Grafting of hexanedithiol to planar gold surfaces

Grafting of hexanedithiol was carried out in aqueous or ethanol solution, at room temperature or at 4 °C. This first step results in some characteristic XPS and PM-IRRAS features: mainly the appearance of an intense S 2p peak on the surface XPS spectra (Fig. 1), and well defined IR absorption bands at 2927 and 2860 cm^{-1} corresponding to the symmetric and asymmetric ν_{CH} in the CH_2 groups of the hexanedithiol chain, respectively (Fig. 2A). Table 1 summarizes the XPS and PM-IRRAS results obtained for various tested experimental conditions. The ratio S/Au, calculated on the basis of XPS results, shown in this table, was considered to compare the amounts of adsorbed dithiols in these different experiments. Thus, working in aqueous media for 12 h led to an S/Au ratio 2.5 times higher than using ethanol as solvent. A similar difference was observed when comparing the CH band areas measured by PM-IRRAS. The area of these bands is expected to increase linearly with the amount of fixed hexanedithiols. Working in aqueous media led to the highest area (Table 1), 2.5 times higher than working in ethanol for the same impregnation time. The thickness of the adsorbed thiol layer was estimated from the decrease of gold signal intensity when compared to a bare gold surface using the following equation:

$$\frac{I(\mathrm{Au}\,4f_{7/2})}{I(\mathrm{Au}\,4f_{7/2})^{\circ}} = \exp\left(-\frac{d}{\lambda_{\mathrm{Au}}\sin\theta}\right) \quad (1)$$

where I(Au $4f_{7/2}$)/I(Au $4f_{7/2}$)° is the Au $4f_{7/2}$ ratio intensity (bare against thiol-functionalized surface), d is the thickness of the organic layer, θ is the take-off angle, fixed at 90°, and λ the escape depth of the Au $4f_{7/2}$ photoelectron trough an organic layer; λ_{Au} = 3.6 nm [27,28].

For a 12 h impregnation in water (S/Au = 0.049), this thickness was close to 2.5 nm, which corresponds to multilayer formation (1 monolayer thickness ~1.2 nm), likely facilitated by interchain hydrophobic interactions. Lowering the immersion time to 3 h, decreased the amount of fixed dithiols for both solvents, and the S/Au ratio obtained in aqueous media (=0.031) was still much higher than that obtained in ethanol. For both solvents, we experienced the sonication of the solutions before immersion and during the rinsing step, but no significant decrease of the S/Au ratio was observed by XPS.

The evolution of the CH band area showed similar tendencies, higher values in water and for long immersion times. The S 2p XPS spectra for various experimental conditions are shown in Fig. 1. On each spectrum, one observes the contribution of two S 2p doublets; the first doublet, at lower binding energy (162 and 163.3 eV for S $2p_{3/2}$ and $2p_{1/2}$ respectively) corresponds to the sulfur bound to gold (Sb), the second, at higher energy (163.6 and 164.9 eV) can be attributed to the sulfur not involved in a covalent bond with gold, but remaining in SH bonds, that we call "free sulfur", Sf. The Sb/Sf ratio, calculated from these data, is also shown in Table 1. This ratio was calculated, taking into account the attenuation of the Sb contribution by the carbon chain, thus using the following equation:

$$I(\mathrm{Sb})\mathrm{cor} = I(\mathrm{Sb}\,\mathrm{exp}) \times \left[\exp\left(-\frac{d_{\mathrm{DT}}}{\lambda_{\mathrm{S}}^{\mathrm{C}}\sin\theta}\right)\right]^{-1} \quad (2)$$

where I(Sb)cor is the value taken to calculate the Sb/Sf ratio, I(Sbexp) is the measured intensity of the low binding energy contribution, d_{DT} is the thickness of the dithiol layer (estimated close to 6 nm), θ is the take-off angle, fixed at 90°, and λ_S^C the escape depth of the S 2p photoelectrons trough the dithiol layer; λ = 3.3 nm. This gives the following result:

$$I(\mathrm{Sb})\mathrm{cor} = I(\mathrm{Sb}\,\mathrm{exp}) \times 1.2$$

The Sb/Sf ratio was considered carefully as a signature of whether dithiols are grafted forming bridges, in an extended configuration, or physically adsorbed. Indeed, if the dithiols are grafted by one single sulfur to the surface, which leaves the second thiol function available to the further grafting of gold nanoparticles, this ratio should be equal to unity; if dithiol molecules form bridges onto the gold surface, Sb/Sf ratio is expected to be higher than 1. Eventually, a Sb/Sf ratio lower than 1 indicates the presence of physically adsorbed dithiols, not involved in covalent bonds with gold, and probably forming multilayers on surfaces. In this case, we may also have bridges hidden by the multilayer, but it is difficult to estimate

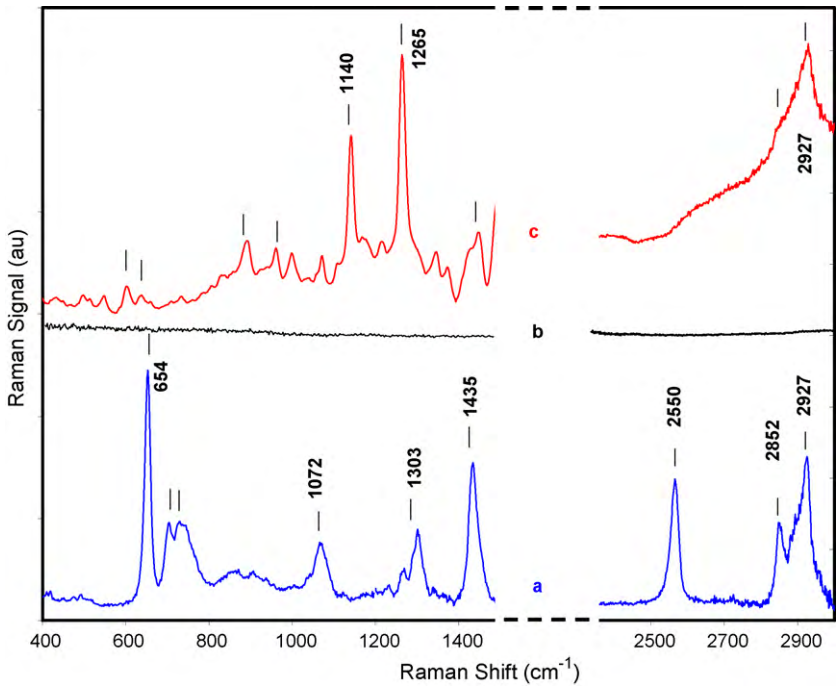

Fig. 3. Raman spectra obtained for: (a) hexanedithiol solution, (b) hexanedithiol grafted on gold, and (c) gold nanoparticles immobilized on an hexanedithiol layer.

their exact amount as the amount of physically adsorbed dithiols is unknown. This latter case was observed when working in aqueous media, which is consistent with the high amount of hexanedithiol determined by XPS and PM-IRRAS. When dithiol attachment was performed in ethanol for 12 h, the Sb/Sf was lower than 1, corroborating the hypothesis of multilayer physisorption. Here again, the results are consistent with both the high S/Au ratio and the measured area of CH IR bands. However, still working in ethanol but after 3 h impregnation, this ratio was equal to 2.2; such a value indicates that the amount of S bound to gold is higher than that of unbound SH groups. The high proportion of bound sulfur can only be explained by the formation of bridges on gold. One can notice, that formation of dithiol bridges occurred at low dithiol coverage (S/Au ratio = 0.006). The same impregnation time but at lower temperature, 4 °C, led to a reasonable amount of adsorbed dithiols. Indeed, the ratio S/Au was equal to 0.01 and the XPS estimated thickness of the layer was close to 1.3 nm, which corresponds to one monolayer with an extended configuration of the grafted species. The Sb/Sf ratio was equal to 1.2, which corroborates these observations.

In conclusion, working in ethanol led to better results than in aqueous media. An impregnation temperature and time of 4 °C and 3 h, respectively, led to the adsorption of one dithiol monolayer with an extended configuration. These conditions were selected to functionalize gold surfaces prior to nanoparticle grafting.

3.2. Grafting of gold nanoparticles to dithiol layer

Before interacting with the thiol layer, the solution of gold nanoparticles was characterized by UV–vis spectroscopy. On the resulting spectrum (see supplementary materials) a narrow plasmon band was present at 525 nm, which corresponds to a homogeneous particle size of ~15 nm [17,23]. The size together with the distribution of the nanoparticles, were also checked by SEM and the images (see supplementary material) corroborated UV–vis data, showing an average particle size of 15 nm and a homogeneous distribution.

Fig. 3 shows the Raman spectra of thiol-functionnalized surfaces before and after deposition of gold nanoparticles (spectra b and c). On this figure is also presented the Raman spectra of a dithiol solution used as reference for dithiol bands (spectrum a). On the dithiol solution spectrum, are present the ν C–S in the 600–800 cm^{-1} region, ν C–C in the 1000–1150 cm^{-1} region, and δ C–H at higher than 1200 cm^{-1}. In the 3000 cm^{-1}, one observes the ν C–H bands around 2900 cm^{-1}. A very intense band at 2550 cm^{-1} is also present and corresponds to the ν S–H vibrations. On the dithiol-terminated layer no signal is recorded as expected from the rather low sensitivity of the Raman spectroscopy on planar surfaces. However, upon nanoparticle grafting, the Raman signal is enhanced due to the plasmon effect of nanoparticles that enables surface enhanced Raman scattering (SERS) [29,30]. The detection of a Raman signal highlights the grafting of gold nanoparticles. On the spectrum of the gold nanoparticle-terminated layer, one can observe the presence of characteristic bands of dithiols already present on the dithiol solution spectrum [31]: ν C–S in the 600–800 cm^{-1} region, ν C–C in the 1000–1150 cm^{-1} region, and δ C–H at higher than 1200 cm^{-1}. Eventually, the ν C–H band at 2927 cm^{-1} is also present but the ν S–H band at 2550 cm^{-1} previously observed for dithiols solution is no more present, proving the covalent grafting of gold nanoparticles by replacing the S–H by S–Au bonds.

Two intense bands, not present in the spectrum of dithiol solution, are also observed at 1140 and 1265 cm^{-1}. These bands are ascribed to the ν C–O vibration of citrates and prove the presence of ligands stabilizing the nanoparticles. The presence of these ligands was also evidenced by PM-IRRAS (Fig. 2B). Indeed, upon the grafting of gold nanoparticles one can observe the IR signal of citrates (ν C=O at 1720 cm^{-1} and ν C–O at 1107 and 1260 cm^{-1}).

Gold nanoparticles dispersion and density were explored by AFM. For these analyses, several experimental parameters were varied. Fig. 4 shows the AFM images obtained after deposition of nanoparticles at room temperature during 1 and 3 h, and at 4 °C during 3 h. An image of the bare gold surface is also shown. One can see that deposition at low temperature led to very few nanoparticles adsorbed as well as the adsorption of some gold aggregates. Conversely, after deposition at room temperature, even during 1 h, the

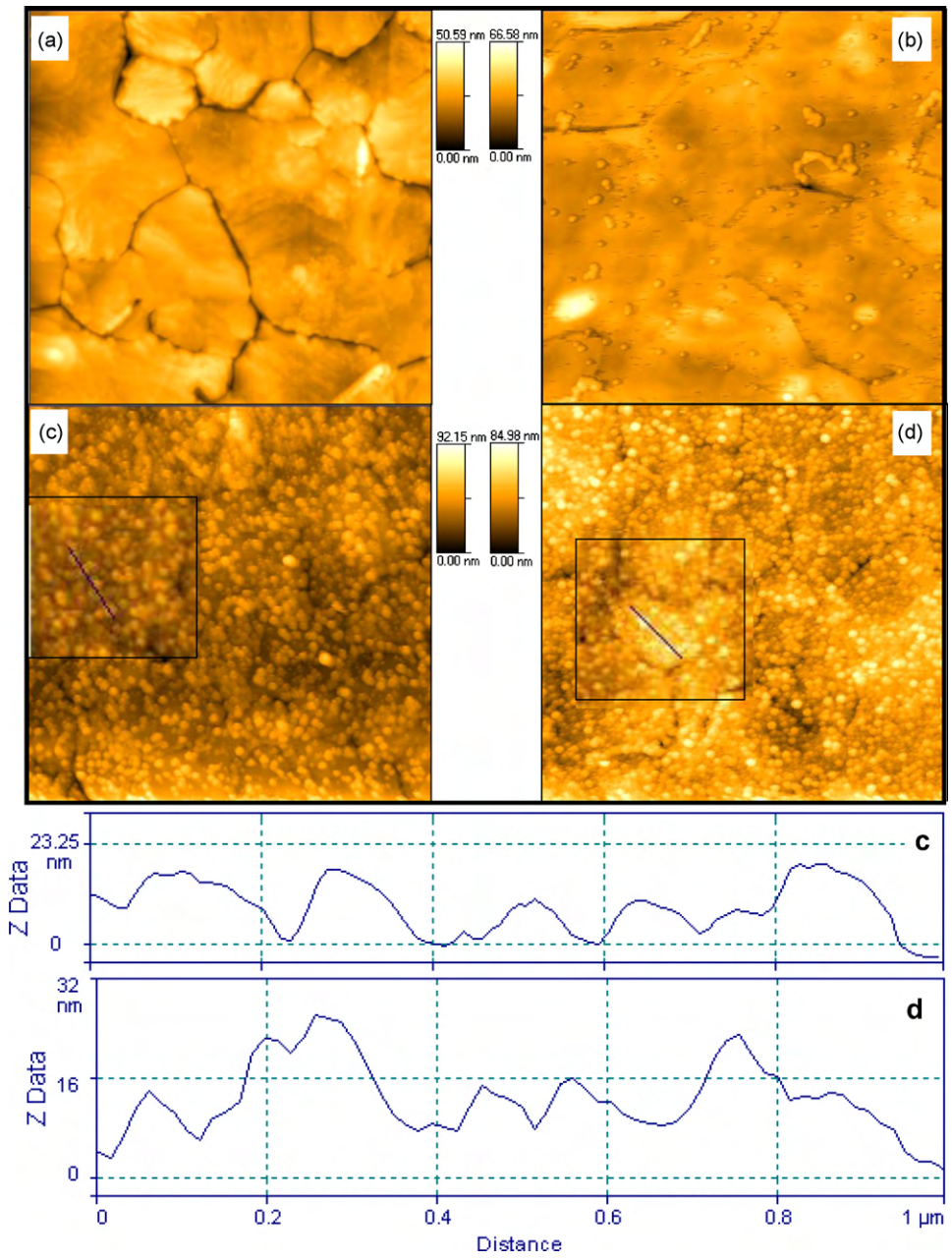

Fig. 4. AFM images (5 μm × 5 μm) of: (a) bare planar gold surface, (b) after deposition of nanoparticles at 4 °C, (c) and (d) after deposition of nanoparticles at room temperature during 1 and 3 h, respectively. Sections of images (c) and (d) are shown.

surface appears to be covered by a much denser layer of nanoparticles. The average thickness of the nanoparticle layer, estimated from 5 images of different zones on the surface, was close to 16 nm, which corresponds to one nanoparticle. Increasing the deposition time led to an increase of the adsorbed amount of nanoparticles; images of various zones revealed height variations of ca. 30 nm suggesting the formation of nanoparticle aggregates.

Sections of images c and d were also shown in Fig. 4, confirming the presence of aggregates of nanoparticles after 3 h of deposition, but not after 1 h. Indeed, Fig. 4c corresponds to a thickness monolayer of 18 nm whereas Fig. 4d shows the thickness of a double layer close to 30 nm. Eventually the nanoparticles coverage on the monolayer of Fig. 4c was evaluated by counting the light spots on a series of five 1 μm × 1 μm images, taking into account the convolution of the AFM tip and was found close to 35% of the planar surface coverage.

XPS spectra of the surface after grafting of nanoparticles were recorded to quantify their density over the dithiol layer; compared to the XPS spectrum of the dithiol-modified surface, a slight increase of the gold peak was observed, which is a complex result of the deposition of nanoparticles and simultaneous attenuation of the planar gold substrate; more interesting, the sulfur peak was significantly attenuated, by a factor close to 25%; this very important result suggests that, even optimizing the deposition conditions, the surface appears to be far from being completely covered with nanoparticles; important to note is that the AFM images, not contradictory to this results but rather due to the tip convolution [32] makes clear a good dispersion of the nanoparticles on the surface. The presence of citrates applies an electrostatic repulsion between nanoparticles preventing a dense coverage to be reached.

Considering these results and having in mind that a rather non-dense layer of nanoparticles is likely favourable to the further

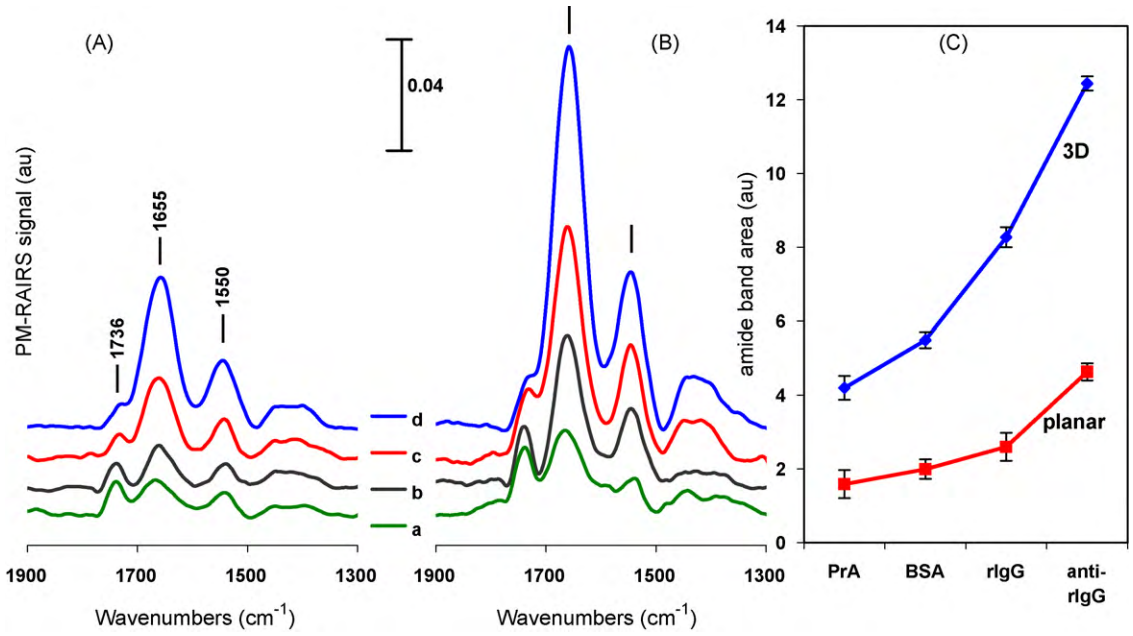

Fig. 5. PM-IRRAS results for planar and 3D immunosensor: (A) and (B) PM-IRRAS spectra after protein A adsorption (a), BSA blocking step (b), rIgG immobilization (c), and anti-rIgG immobilization (d). (C) The corresponding integration of amide band areas.

binding of proteins, the chosen conditions for nanoparticle immobilization were room temperature and 1 h impregnation time.

3.3. Building of the model 3D immunosensor

3D immunosensors were elaborated on the previously optimized gold nanoparticle-modified surface. This 3D layer and the planar gold surface were treated under exactly the same conditions along all the successive steps of the immunosensor elaboration, the planar gold surface being considered as a planar "reference" sample. Both surfaces were first functionalized by MUA (mercaptoundecanoic acid), then, after an activation step, PrA (Protein A) was covalently linked *via* its amine groups. Note that, on citrate-stabilized nanoparticles, strongly binding MUA thiols are expected to replace, at least partially, the citrate ligands [33]. To block non-specific adsorption sites, BSA was added. A model rabbit immunoglobulin (rIgG) was then immobilized by bioaffinity on the PrA layer. Since this model antibody is not directed against a specific target, the reactivity of immunosensors was indirectly estimated by measuring the antibody accessibility; this was achieved by submitting the sensing layers to a solution containing a secondary antibody, a goat anti-rIgG. We also checked the specificity of the so-obtained immunosensors by depositing a goat serum and checking whether proteins were adsorbed or not. Each of the mentioned steps was characterized by PM-IRRAS for both planar and 3D immunosensors. Surface enhanced Raman scattering was also utilized at each of these steps. However, the resulting spectra exhibited a multitude of peaks whose intensities and related intensities were dependant on the position of the laser beam. Moreover, the decrease of the SERS effect with distance [30] makes the quantification of adsorbed proteins difficult. We are now working on the better interpretation of SERS data. At that point, we will focus our attention on PM-IRRAS data that enable a reliable quantitative comparison of substrate performances.

Fig. 5 shows the PM-IRRAS spectra obtained during the elaboration and test of the planar and 3D immunosensors. One can observe intense amide bands, characteristic of protein adsorption: amide I at 1655 cm^{-1} corresponds to ν C=O vibration, amide II at 1550 cm^{-1} due to the coupled C–N stretching and N–H bending modes. A third band located at 1736 cm^{-1}, due to residual ester functions, is also present. These functions could be reduced using ethanolamine for example. In our case, we observed that this reduction has no dramatic influence neither on the amount of adsorbed BSA nor on the specificity of the sensing layer, probably because these functions are hidden by adsorbed proteins. We thus suppress that reduction step; however, we included this band when integrating and discussing amide band areas.

Amide band areas increased at each step of protein adsorption. We previously evidenced a direct correlation between the amount of adsorbed proteins and the area of these two bands [34]. Moreover, when the resulting amide band areas are corrected by the molecular weight for each protein, one can advantageously compare the immobilized molecular amounts of the various proteins [7]. These data are shown in Fig. 5 for both planar and 3D immunosensors. Passing from the planar to the 3D sensing surface, the molecular amount of protein A was doubled, even taking into account the higher experimental error bars recorded for the latter surface at this step. On the planar sensors, the amount of PrA is 5 times higher than that of BSA. Considering the areas occupied by these two proteins, ~20 and 56 nm^2 ([7] and references therein) for PrA and BSA, respectively, this ratio corresponds to 60% of the surface covered with PrA and 40% with BSA, in agreement with previously elaborated systems [35]. For the 3D sensors, the molecular PrA/BSA ratio was lower, ~3, which corresponds to a 50% surface occupancy by each protein.

On each PrA, twice as much rIgGs were immobilized on 3D compared to planar immunosensors, proving their enhanced accessibility. This result is very satisfying as the increase in specific surface area upon the immobilization of 15 nm nanoparticles is not that important; nanoparticles being spherical, 25% of the surface coverage leads to a final surface area of 125% of the planar one. Such an increase is probably accompanied by a gain of accessibility and also flexibility of the gold surface.

The specificity of the sensing layers was tested with a goat serum solution. On either the planar or the 3D sensor, amide band areas were not modified indicating the absence of non-specific protein interactions, likely due to the efficient blocking step by BSA. The accessibility of these rIgG was checked to see whether increasing

their amount create or not steric hindrance that could lower their activity. The question is now whether binding a higher amount of antibodies tends to modify, and in which direction, their accessibility. On planar sensors, the anti-rIgG/rIgG ratio was between 2 and 3, which indicates a very high accessibility of the immobilized antibodies. On 3D immunosensors, this ratio was slightly reduced, down to ca. 2; this value is still high. Indeed, the used secondary antibody, anti-rIgG recognizes the constant fragment of the immobilized rIgG; these rIgG being immobilized on protein A through the same fragment, at the bottom of the "Y", the Fc is the less accessible receptors part, and a factor of almost 2 is still very satisfying! Thus, despite the small number of nanoparticles, the objective of increasing the antibody density while preserving a satisfying accessibility was reached. One reason for that may be the increase of flexibility of the sensing layer when compared to planar sensor; on going experiments, using QCM-D (quartz crystal microbalance with dissipation measurement), aim at determining the exact change in viscoelastic properties of the sensing layer between the planar and the 3D immunosensors. Another considerable increase in sensitivity is expected by using SPR as transducing technique as, besides the increase of rIgGs already observed by PM-IRRAS, SPR will benefit from the plasmon effect of nanoparticles and an enhancement of one order magnitude could be expected [36,37]. Work on optimization of nanogold grafting on SPR-chips is already in progress.

4. Conclusion

In this study, grafting of alkyldithiols onto planar gold substrates was investigated and monitored by PM-IRRAS and XPS at various experimental conditions. These conditions were optimized to ensure the best grafting of these molecules i.e.: an ordered monolayer with an S bound to gold and a second S free to ensure covalent immobilization of gold nanoparticles. This immobilization was also optimised and we were able to build up a 3D gold platform with a well dispersed monolayer of gold nanoparticles. This platform was then used to elaborate a model 3D immunosensor and compare it, in terms of molecular accessibility, to planar sensors; PM-IRRAS spectra highlighted the possibility to increase the number of receptors by a factor of 4, while preserving a good accessibility.

This approach will be developed and optimised to design arrays of nanoparticles that should enable the binding of a large number of antibodies and benefit of the signal enhancement in SPR and IR surface spectroscopies.

Appendix A. Supplementary data

Supplementary data associated with this article can be found, in the online version, at doi:10.1016/j.colsurfb.2010.07.021.

References

[1] R.F. Taylor, J.S. Schultz (Eds.), Handbook of Chemical and Biological Sensors, 1996.
[2] P.B. Luppa, L.J. Sokoll, D.W. Chan, Immunosensors—principles and applications to clinical chemistry, Clinica Chimica Acta 314 (2001) 1–26.
[3] M. Campas, B. Prieto-Simon, J.-L. Marty, Biosensors to detect marine toxins: assessing seafood safety, Talanta 72 (2007) 884–895.
[4] E. Delibato, M. Bancone, G. Volpe, D. De Medici, D. Moscone, G. Palleschi, Development and comparative evaluation of different screening methods for detection of *Staphylococcus aureus*, Analytical Letters 38 (2005) 1569–1586.
[5] S. Boujday, R. Briandet, M. Salmain, J.-M. Herry, P.-G. Marnet, M. Gautier, C.-M. Pradier, Detection of pathogenic *Staphylococcus aureus* bacteria by gold based immunosensors, Microchimica Acta 163 (2008) 203–209.
[6] S. Boujday, C. Gu, M. Girardot, M. Salmain, C.-M. Pradier, Surface IR applied to rapid and direct immunosensing of environmental pollutants, Talanta 78 (2009) 165–170.
[7] S. Boujday, A. Bantegnie, E. Briand, P.-G. Marnet, M. Salmain, C.-M. Pradier, In-depth investigation of protein adsorption on gold surfaces: correlating the structure and density to the efficiency of the sensing layer, Journal of Physical Chemistry B 112 (2008) 6708–6715.
[8] B. Kasemo, Biological surface science, Surface Science 500 (2002) 656–677.
[9] N.K. Chaki, K. Vijayamohanan, Self-assembled monolayers as a tunable platform for biosensor applications, Biosensors and Bioelectronics 17 (2002) 1–12.
[10] E. Briand, C. Gu, S. Boujday, M. Salmain, J.-M. Herry, C.M. Pradier, Functionalisation of gold surfaces with thiolate SAMs: topography/bioactivity relationship—a combined FT-RAIRS, AFM and QCM investigation, Surface Science 601 (2007) 3850–3855.
[11] S. Ko, T.J. Park, H.-S. Kim, J.-H. Kim, Y.-J. Cho, Directed self-assembly of gold binding polypeptide-protein A fusion proteins for development of gold nanoparticle-based SPR immunosensors, Biosensors and Bioelectronics 24 (2009) 2592–2597.
[12] H. Wang, J. Wu, J. Li, Y. Ding, G. Shen, R. Yu, Nanogold particle-enhanced oriented adsorption of antibody fragments for immunosensing platforms, Biosensors and Bioelectronics 20 (2005) 2210–2217.
[13] L.A. Lyon, M.D. Musick, M.J. Natan, Colloidal Au-enhanced surface plasmon resonance immunosensing, Analytical Chemistry 70 (1998) 5177–5183.
[14] S. Zhang, N. Wang, H. Yu, Y. Niu, C. Sun, Covalent attachment of glucose oxidase to an Au electrode modified with gold nanoparticles for use as glucose biosensor, Bioelectrochemistry 67 (2005) 15–22.
[15] J.W. Choi, D.-Y. Kang, Y.-H. Jang, H.-H. Kim, J. Min, B.-K. Oh, Ultra-sensitive surface plasmon resonance based immunosensor for prostate-specific antigen using gold nanoparticle–antibody complex, Colloids and Surfaces A: Physicochemical and Engineering Aspects 313–314 (2008) 655–659.
[16] C.-C. Lin, Y.-M. Yang, Y.-F. Chen, T.-S. Yang, H.-C. Chang, A new PrA assay based on Raman reporter labeled immunogold nanoparticles, Biosensors and Bioelectronics 24 (2008) 178–183.
[17] O. Seitz, M.M. Chehimi, E. Cabet-Deliry, S. Truong, N. Felidj, C. Perruchot, S.J. Greaves, J.F. Watts, Preparation and characterisation of gold nanoparticle assemblies on silanised glass plates, Colloids and Surfaces A: Physicochemical and Engineering Aspects 218 (2003) 225–239.
[18] Z. Zhong, S. Patskovskyy, P. Bouvrette, J.H.T. Luong, A. Gedanken, The surface chemistry of Au colloids and their interactions with functional amino acids, Journal of Physical Chemistry B 108 (2004) 4046–4052.
[19] Y.Y. Xu, C. Bian, S. Chen, S. Xia, A microelectronic technology based amperometric immunosensor for fetoprotein using mixed self-assembled monolayers and gold nanoparticles, Analytica Chimica Acta 561 (2006) 48–54.
[20] Z. Liu, J. Liu, G. Shen, R. Yu, A reagentless tyrosinase biosensor based on 16-hexanedithiol and nano-Au self-assembled monolayers, Electroanalysis 18 (2006) 1572–1577.
[21] Y. Joseph, I. Besnard, M. Rosenberger, B. Guse, H.-G. Nothofer, J.M. Wessels, U. Wild, A. Knop-Gericke, D. Su, R. Schlo, A. Yasuda, T. Vossmeyer, Self-assembled gold nanoparticle/alkanedithiol films: preparation, electron microscopy, xps-analysis, charge transport, and vapor-sensing properties, Journal of Physical Chemistry B 107 (2003) 7406–7413.
[22] G Shen, H. wang, G. Shen, R. Yu, Au nanoparticle network-type thin films formed via mixed assembling and cross-linking route for biosensor application: quartz crystal microbalance study, Analytical Biochemistry 365 (2007).
[23] J. Turkevich, J. Hillier, P.C. Stevenson, A study of the nucleation and growth processes in the synthesis of colloidal gold, Discussions of the Faraday Society 11 (1951) 55.
[24] E. Briand, Fonctionnalisation de Surfaces d'Or et greffage de protéines pour l'élaboration d'un immunocapteur, Doctorat d'Université, UPMC, Paris, 2007.
[25] B.J. Barner, M.J. Green, E.I. Saez, R.M. Corn, Polarization modulation Fourier transform infrared reflectance measurements of thin films and monolayers at metal surfaces utilizing real-time sampling electronics, Analytical Chemistry 63 (1991) 55–63.
[26] T. Buffeteau, B. Desbat, J.M. Turlet, Polarization modulation FT-IR spectroscopy of surfaces and ultra-thin films: experimental procedure and quantitative analysis, Applied Spectroscopy 45 (1991) 380–389.
[27] C.D. Bain, G.M. Whitesides, Attenuation lenghts of photoelectron in hydrocarbon films, Journal of Physical Chemistry 93 (1989) 1670–1673.
[28] P.E. Laibinis, C.D. Bain, G.M. Whitesides, Attenuation of photoelectrons in monolayers of n-alkanethiols adsorbed on copper, Journal of Physical Chemistry 95 (1991).
[29] M. Moskovits, Surface-enhanced Raman spectroscopy: a brief retrospective, Journal of Raman Spectroscopy 36 (2005) 485–496.
[30] Z.Q. Tian, Surface-enhanced Raman spectroscopy: advancements and applications, Journal of Raman Spectroscopy 36 (2005) 466–470.
[31] N. Sandhyarani, T. Pradeep, Characteristics of alkanethiol self assembled monolayers prepared on sputtered gold films: a surface enhanced Raman spectroscopic investigation, Vacuum 49 (1998) 2279–2284.
[32] D. Keller, Reconstruction of STM and AFM images distorted by finite-size tips, Surface Science 253 (1991) 353–364.
[33] A. Bonifacio, L. van der Sneppen, C. Gooijer, G. van der Zwan, Citrate-reduced silver hydrosol modified with ω-mercaptoalkanoic acids self-assembled monolayers as a substrate for surface-enhanced resonance Raman scattering. A study with cytochrome c, Langmuir 20 (2004) 5858–5864.

[34] S. Boujday, C. Methivier, B. Beccard, C.-M. Pradier, Innovative surface characterization techniques applied to immunosensor elaboration and test: comparing the efficiency of FT-SPR, QCM-D, and PM-IRRAS, Analytical Biochemistry 387 (2009) 194–201.
[35] E Briand, C. Gu, S. Boujday, M. Salmain, J.M. Herry, C.M. Pradier, Functionalization of gold surfaces with thiolate SAMs: topography/bioactivity relationship—a combined FT-RAIRS, AFM and QCM investigation, Surface Science 601 (2007) 3850–3855.
[36] X.D. Hoa, A.G. Kirk, M. Tabrizian, Enhanced SPR response from patterned immobilization of surface bioreceptors on nano-gratings, Biosensors and Bioelectronics 24 (2009) 3043–3048.
[37] H. Tanakaa, M. Hanasakib, T. Isojimab, H. Takeuchib, T. Shiroyab, H. Kawaguchi, Enhancement of sensitivity of SPR protein microarray using a novel 3D protein immobilization, Colloids and Surfaces B: Biointerfaces 70 (2009) 259–265.